






## Research Article

# Numerical Study of Carbon Nanofoam Targets for Laser-Driven Inertial Fusion Experiments

A. Maffini <sup>1</sup>, M. Cipriani <sup>2</sup>, D. Orecchia,<sup>1</sup> V. Ciardiello,<sup>1,2</sup> A. Formenti,<sup>1</sup> F. Consoli <sup>2</sup>  
 and M. Passoni<sup>1</sup>

<sup>1</sup>Energy Department, Politecnico di Milano, Piazza Leonardo da Vinci 33, Milan 20133, Italy

<sup>2</sup>ENEA, Fusion and Technologies for Nuclear Safety Department, C.R. Frascati, Frascati 00044, Italy

Correspondence should be addressed to A. Maffini; [alessandro.maffini@polimi.it](mailto:alessandro.maffini@polimi.it) and M. Cipriani; [mattia.cipriani@enea.it](mailto:mattia.cipriani@enea.it)

Received 11 March 2023; Revised 20 June 2023; Accepted 15 July 2023; Published 2 September 2023

Academic Editor: Yuji Fukuda

Copyright © 2023 A. Maffini et al. This is an open access article distributed under the Creative Commons Attribution License, which permits unrestricted use, distribution, and reproduction in any medium, provided the original work is properly cited.

Porous materials have peculiar characteristics that are relevant for inertial confinement fusion (ICF). Among them, chemically produced foams are proved to be able to smooth the laser inhomogeneities and to increase the coupling of the laser with the target. Foams realized with other elements and techniques may prove useful as well for ICF applications. In this work, we explore the potential of a novel class of porous materials for ICF, namely, carbon nanofoams produced with the pulsed laser deposition (PLD) technique, by means of hydrodynamic numerical simulations. By comparison with a simulation of solid-density carbon, PLD nanofoams show a higher pressure at the shock front, which could make them potential good candidates as ablaters for a capsule for direct-drive fusion.

## 1. Introduction

Porous materials, or foams, are the subject of an intense research activity in the context of inertial confinement fusion (ICF) and, more generally, of laser-matter interaction. Foams of low-Z elements have been proposed for use in ICF capsules, to generate bright X-ray sources [1], for the study of equations of state [2], and more recently for efficient electron acceleration [3].

In the context of ICF, foams are considered as constituents of the outer layer of the capsule, because of their ability to smooth the inhomogeneities in the laser energy [4–7], to enhance the laser absorption efficiency [8, 9], and to increase the ablation loading on a substrate [10]. These features make a foam ablator a potentially important choice to increase the laser-target coupling, thus transferring the laser energy into compression of the inner layers of the capsule.

Most of the experimental data available regard plastic foams, whose internal structure is constituted by features in the micrometric scale, such as filaments and membranes.

Typically, these foams are produced by chemical methods. However, the investigation of the behavior of porous materials constituted by different elements and materials is needed to explore other potential applications. Recent studies [11, 12] indicate the advantages of using mid-Z ablaters, which can reduce the impact of laser plasma instabilities (LPIs), therefore increasing the performance of the target. Among them, high-density carbon (HDC), typically used in indirect-drive experiments, can be beneficial for enhancing the performances of capsules, not only for the indirect-drive scheme but also for the direct-drive approach. In this context, low-density carbon nanofoams could potentially combine the benefits coming from the use of an ablator made of mid-Z elements and from the features of plasma behavior deriving from its random internal structure.

In this work, we present the first numerical investigation of the behavior of nanostructured carbon foams produced with the pulsed laser deposition (PLD) technique [13–15] under the action of a high-power nanosecond-long laser beam, at conditions relevant to ICF. PLD nanofoams have

already been studied in the framework of high-intensity laser-matter interaction as a near-critical layer in double-layer targets [16] for ion acceleration with ultrafast lasers (pulse duration from  $\sim 30$  fs to 100s fs) [17, 18].

In this context, a solid theoretical understanding of the physical processes granting an enhanced acceleration has been developed thanks to particle-in-cell kinetic simulations [19–21], and the optimal nanofoam parameters (namely, thickness and density) have been determined as a function of laser intensity [22]. However, there are significant differences in the laser parameters between typical ultrafast laser-driven acceleration and ICF experiments, especially in terms of pulse duration (typically from 30 fs to 100s fs for the former, few ns for the latter) and irradiance (typically  $10^{18}$ – $10^{22}$  W/cm<sup>2</sup> and  $10^{14}$ – $10^{15}$  W/cm<sup>2</sup>, respectively), and dedicated studies are thus required. Particle-in-cell codes are not suited to simulate dynamical processes evolving on the longer timescales relevant for ICF (up to hundreds of nanoseconds).

Here, we use the hydrodynamic MULTI-FM code [23], validated with experiments on microstructured plastic foams [24], to simulate the behavior of the PLD carbon nanofoams. The need for a dedicated code has been confirmed in the last years since modeling the foam as an equivalent medium of the same density in the simulations proved to be unsatisfactory [6, 23]. The MULTI-FM code features a model for reproducing the laser absorption in the foam and the behavior of the laser-generated plasma, by taking into account the randomly arranged internal structure of the material.

We consider a set of different nanofoam parameters, which depend on the manufacturing process used and in particular on the time duration of the laser employed. From the simulations, we find that the shockwave in all the foams is significantly slower than in a homogeneous medium with the same density as the nanofoam, as expected from the studies with the plastic foams [24, 25]. Moreover, we find the indication that the pressure at the front of the shockwave is significantly larger than the one obtained in the equivalent homogeneous medium.

## 2. Methods

**2.1. Materials.** The carbon nanofoam presented in this work is produced by pulsed laser deposition (PLD), a physical vapour deposition technique that employs a pulsed laser to remove material from a target and deposit it on a substrate in a controlled gas atmosphere. If the background gas pressure is sufficiently high with respect to the energy of the ablated species, they can be slowed to a diffusive regime and aggregate while in flight, giving rise to porous, nanostructured, low-density films. In the case of carbon, what can be obtained are carbon nanofoams, nanoparticle-assembled films with a fractal-like morphology, whose basic constituents are nanoparticles with dimensions in the order of 10 nm and densities as low as a few mg/cm<sup>3</sup>.

Two different deposition systems are employed, one exploiting a nanosecond duration laser (ns-PLD, conventional technique) and the other an ultrashort femtosecond

laser (fs-PLD). The first is a Q-switched Nd:YAG laser (second harmonic  $\lambda = 532$  nm), with 5–7 ns pulse duration, 1 J maximum pulse energy, 10 Hz repetition rate; the second is a Ti:sapphire-based CPA laser (Coherent Astrella,  $\lambda = 800$  nm),  $\sim 100$  fs pulse duration, 5 mJ maximum pulse energy, 1 kHz repetition rate. As shown in previous work [15], the different laser pulse duration leads to very different ablation regimes and enables better control of the foam properties. Notably, carbon nanofoams with the same density and different spatial uniformity (i.e., different microscale homogeneity) can be obtained.

The PLD target is pyrolytic graphite, the laser incidence angle is 45°, and the distance between target and substrate is fixed at 7 cm. We set the fluence to 360 mJ/cm<sup>2</sup> for both techniques, obtained with 8 mm spot size (top hat) and 260 mJ for ns-PLD and 0.8 mm spot size (FWHM) and 2.6 mJ for fs-PLD. By suitably tuning the vacuum chamber pressure in the range from 50 to 200 Pa (argon is used as an inert gas), carbon nanofoams of different densities are obtained. Combining the effect of the pressure with the effect of the different techniques (ns-PLD and fs-PLD), four kinds of representative carbon nanofoam are produced, as shown in Table 1.

The nanofoam morphology is characterized with a field emission scanning electron microscope (SEM, Zeiss Supra 40) with 3–10 kV accelerating voltage. The microscope electron is also exploited to perform EDXS (energy-dispersive X-rays spectroscopy) on the foam samples and to obtain information about the elemental composition and average density. This is done through the EDDIE method [26]: a theoretical model of the electron transport in the film and substrate allows to retrieve the film mass thickness starting from the ratio between the respective X-rays line intensities. The nanofoam thickness is measured from the SEM cross-sectional images, and the density is obtained as their ratio.

The determination of the nanofoam pore size  $\delta_0$ , one of the parameters needed for the foam model implemented in the MULTI-FM code, is not straightforward: contrary to most of the chemically produced foams, pulsed laser-deposited nanofoams are cluster-assembled and fractal, with disordered voids without a clear shape. One possibility is to estimate the average pore size with the characteristic uniformity scale length of the nanofoam, that is, the average distance between two adjacent high-density regions of the foam (or equivalently the distance between two less-dense regions, i.e., the void dimension). The EDDIE method can be used point-by-point on the samples to build mass thickness maps of the foams, and by performing a Fourier transform analysis on the maps, the nanofoam uniformity scale length is obtained. In principle, it would be possible to perform the Fourier transform analysis directly on the SEM images, but they would be affected by electronic effects and arbitrary postprocessing (i.e., contrast and brightness), while the mass thickness maps cleanly convey the useful physical information. The structure factor  $S(q)$  is the radius-averaged squared Fourier transform of the mass thickness image, and since the spatial frequency

TABLE 1: The parameters of the materials produced with the PLD. The solid element density  $\rho_s$  is taken as  $2.0 \text{ g/cm}^3$  for all samples.

Series	Deposition method	Density $\rho_p$ ( $\text{mg/cm}^3$ )	$\delta_0$ ( $\mu\text{m}$ )	$b_0$ (nm)
A	ns-PLD	6	10	30
B	fs-PLD	6	20	60
C	ns-PLD	18	5	45
D	fs-PLD	18	10	90

$q_{\text{max}}$ —corresponding to the maximum value of  $S(q)$ —is the predominant spatial frequency in the image, its inverse ( $1/q_{\text{max}}$ ) is the uniformity scale length [15], and that value is used as an estimate for  $\delta_0$ .

Four distinct categories of carbon nanofoams are produced and investigated in this work, as reported in Table 1: sample Figures 1(a) and 1(b) have a density of  $6 \text{ mg/cm}^3$ , which is the characteristic lowest carbon nanofoam density achievable with the PLD technique; sample Figures 1(c) and 1(d) are three times as dense ( $18 \text{ mg/cm}^3$ ), close to the highest density conditions in which the material retains a porous, foam-like structure. For each density, the samples produced with ns-PLD (Figures 1(a) and 1(c)) present a pore size that is half of the value obtained for corresponding fs-PLD samples (Figures 1(b) and 1(d)). This can be appreciated from Figure 1: Figures 1(a) and 1(d) are similar in the distance between two crests of the microscale foam structure, and Figure 1(b) has a greater spacing while Figure 1(c) is significantly more uniform. Figure 2 shows the respective EDXS mass thickness maps, highlighting the same nanofoam microstructure. From the Fourier transform image in the insets, the ring at  $q_{\text{max}}$  can be appreciated (note the wider scale for the Figure 1(c) inset).

Since carbon nanofoams grow through the random stacking of aggregates which are fractal in nature, it is possible to relate the density of the nanofoams to the characteristics of the fractal aggregates [15]:

$$\frac{\rho_p}{\rho_s} = k \left( \frac{d_{np}}{2R_g} \right)^{3-D_f}, \quad (1)$$

where  $\rho_p$  and  $\rho_s$  are, respectively, the foam and the solid element (nanoparticle) density and  $k$  is a proportionality factor related to the packing of the aggregates in the three-dimensional foam structure.  $d_{np}$ ,  $R_g$ , and  $D_f$  are the fractal aggregates properties: nanoparticle diameter, gyration radius, and fractal dimension. Since all the carbon nanofoams considered in this work have a fractal dimension  $D_f \approx 2$  [15],

$$\frac{\rho_p}{\rho_s} = k \left( \frac{d_{np}}{2R_g} \right) = \left( \frac{d_{np}}{(2R_g/k)} \right). \quad (2)$$

The foam model implemented in the MULTI-FM code is still based on a fractal description but expresses the  $\rho_p$  over  $\rho_s$  ratio as a function of different parameters: the thickness of the solid elements  $b_0$ , the pore size  $\delta_0$ , and the fractal parameter  $\alpha$ .

$$\frac{\rho_p}{\rho_s} = \left( \frac{b_0}{\delta_0} \right)^{1/\alpha}. \quad (3)$$

By comparing the two equations, one could seek a way to express each term of (3) as a function of the parameters of the other, namely,  $d_{np}$ ,  $2R_g$ , and  $D_f$ , since the left-hand term is the same in both equations. Given the number of parameters and their possible combinations, a complete term-by-term correspondence is not univocal. A very straightforward relationship between  $\alpha$  and  $D_f$  can be derived, as they are both a measure of the fractality of the system, and it is reasonable to assume they should be independent of the other parameters. Under this hypothesis, equating the exponents of the two equations leads to  $\alpha = (3 - D_f)^{-1} \approx 1$ . Then, since the pore dimension  $\delta_0$  is obtained from the Fourier analysis of the mass thickness maps, the only remaining parameter  $b_0$  can be calculated by inverting (3):  $b_0 = ((\rho_p/\rho_s) \cdot \delta_0)^\alpha = (\rho_p/\rho_s) \cdot \delta_0$ . A value of  $2.0 \text{ g/cm}^3$  is taken as solid element density  $\rho_s$ , coherent with the disordered  $\text{sp}^2$  structure of the carbon nanoparticles composing the nanofoam [13, 14, 27]. The main parameters for the different carbon nanofoams considered in this study (Series A, B, C, and D) are shown in Table 1: their density, pore dimension  $\delta_0$ , and solid element dimension  $b_0$ , along with the respective production technique (ns- or fs-PLD). It can be noted that the value of the solid element thickness  $b_0$ , in the order of some tens of nanometers, is coherent with the foam microstructure as seen in high magnification SEM images. Since the nanoparticle diameter is around 10 nm, the carbon nanofoam solid element can be identified with the strands of connected nanoparticles that make up the short-range structure of the nanofoams, which delimit the voids—of dimension  $\delta_0$ —from one another. Therefore, the foam model implemented in MULTI-FM is representative of the nanofoam microstructure, while it is not sensitive to the short-range nanostructure (namely, the nanoparticles composing the foam solid element).

**2.2. MULTI-FM Simulations.** We simulated the behavior of the laser-generated plasma with the 1D MULTI-FM code [23]. The MULTI-FM code is a modification of the MULTI code [28] specifically developed for reproducing the interaction of powerful laser pulses with porous materials. It is based on an effective model for laser absorption accounting for the effect of solid elements and empty spaces on the plasma behavior. In the model, the pore size  $\delta_0$ , the thickness of the solid elements  $b_0$ , the average density of the foam  $\rho_p$ , and the density of the solid parts  $\rho_s$  are related as in equation (3). In the code, the homogenization status of the plasma is determined through a parameter called ISFOAM, defined for each numerical cell at each time step as

$$\text{ISFOAM}(x, t) = 1 - \frac{H(x, t)}{H_c}. \quad (4)$$

In this equation,



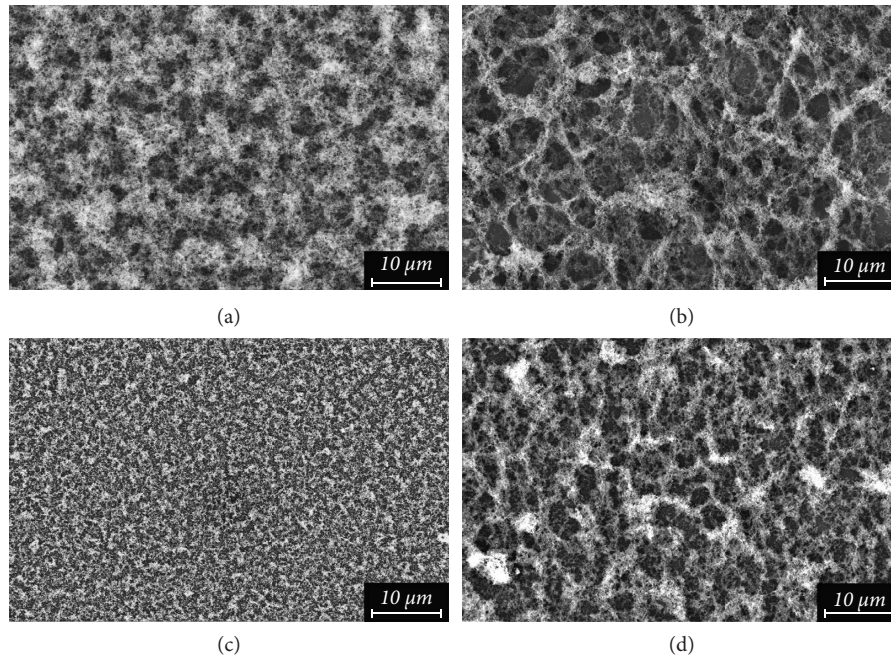


FIGURE 1: SEM micrographs of the carbon nanofoams produced. The respective properties can be found in Table 1 for the (a), (b), (c), and (d) samples. The images can be directly compared since the magnification is the same in all cases.

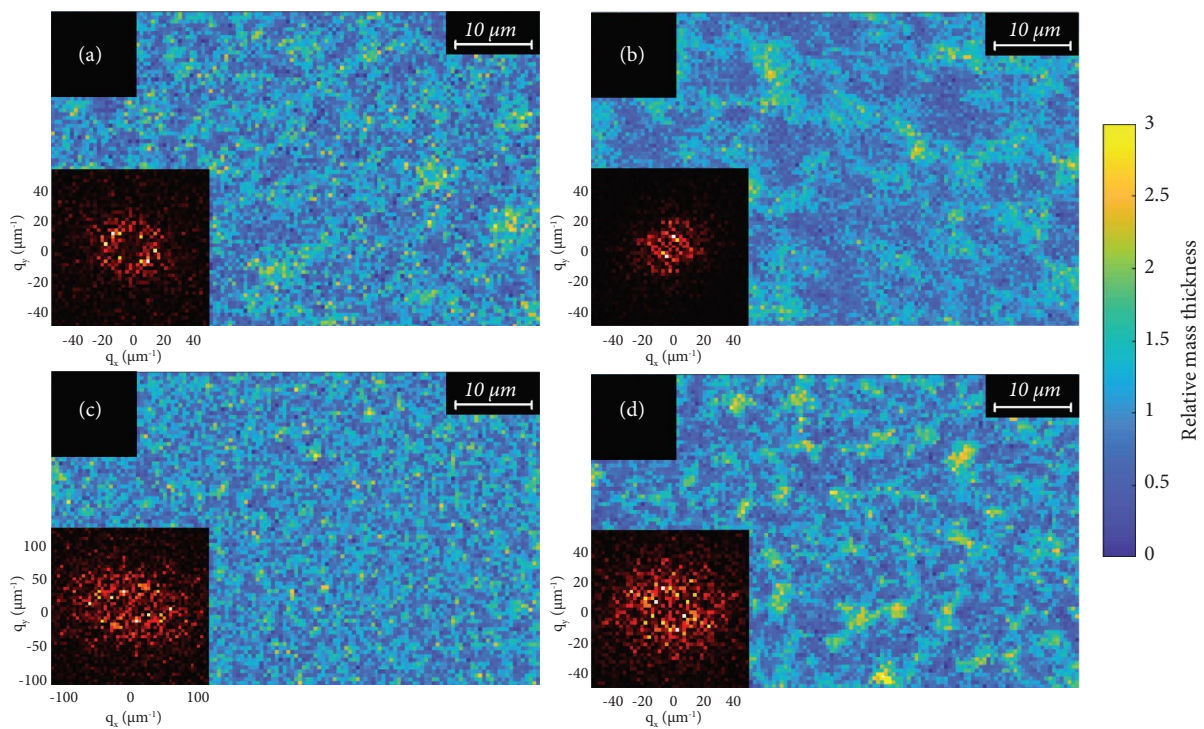


FIGURE 2: Mass thickness maps of the carbon nanofoam samples from Figure 1. In the inserts on the lower left, the Fourier transform of the respective image is shown. The anticorrelation between uniformity scale and maximum  $q$  can be appreciated (note the different scale of the inset of figure (c)).

$$H(x, t) = 2 \int_0^t \frac{dt'}{\tau_H(x, t')}, \quad (5)$$

where  $\tau_H$  is the characteristic homogenization time given as follows:

$$\begin{aligned} \tau_H &\approx 2.4 \cdot 10^{-3} \frac{Z^4 (\delta_0 - b_0)^2 \rho_p}{A^{(1/2)} T^{(5/2)}} \\ &= 2.4 \cdot 10^{-3} \frac{Z^4 \delta_0^2 [1 - (\rho_p/\rho_s)]^{\alpha^2} \rho_p}{A^{(1/2)} T^{(5/2)}}, \end{aligned} \quad (6)$$

where  $Z$  is the effective ionization,  $A$  is the mass number, and  $T$  is the temperature of the plasma. In the last step, equation (3) was substituted in place of  $b_0$  to better illustrate the dependence of the homogenization time on pore dimension and density. Due to the low density of the nanofoams,  $(\rho_p/\rho_s) \ll 1$ , therefore,  $\tau_H \propto \delta_0^2 \rho_p$ . When the homogenization is reached,  $H(x, t_h)$  is

$$H(x, t_h) = H_c = \begin{cases} 1, & \rho_p \geq \rho_c, \\ 1 - \left[ \frac{1 - (\rho_p/\rho_c)^\alpha}{1 - (\rho_p/\rho_s)^\alpha} \right]^2, & \rho_p < \rho_c. \end{cases} \quad (7)$$

As the plasma is heated and homogenized, the parameter ISFOAM changes from 1 for the cold, not yet irradiated foam, to 0, when the plasma in the cell is completely homogenized. In the model, the thermal conduction is limited by the same parameter ISFOAM, to account for the inhomogeneous distribution of free electrons in the pores during homogenization as follows:

$$q(x, t) = -(1 - \text{ISFOAM}(x, t)) \left[ \chi(x, t) \frac{\partial T_e}{\partial x} \right], \quad (8)$$

where  $q(x, t)$  is the heat flux,  $\chi(x, t)$  is the Spitzer conductivity, and  $T_e(x, t)$  is the electron temperature. In the same fashion, the force acting on the mesh nodes is limited by the homogenization as

$$\frac{\partial v}{\partial t} = -(1 - \text{ISFOAM}(x, t)) \frac{\partial P}{\partial m}, \quad (9)$$

where  $v(x, t)$  is the node velocity,  $P(x, t)$  is the total pressure, and  $m$  is the Lagrangian coordinates used in the calculations in the code.

The MULTI-FM code has been validated with an experimental campaign carried out at the ABC laser facility [24].

Here, the laser parameters are taken as the ones of the ABC laser facility, in view of an experimental campaign to be conducted there in the near future. The laser pulse has a  $\sin^2$  temporal profile with a full-width half maximum (FWHM)  $\tau_L = 3$  ns, at the fundamental wavelength  $\lambda_L = 1054$  nm, with an intensity on target of  $10^{14}$  W/cm<sup>2</sup>. The parameters for the carbon nanofoam samples used in the simulations are

the ones indicated in Table 1. In all the simulations, a tabulated equation of state from the SESAME library has been used. The carbon ions are considered to be fully ionized,  $Z_{\text{eff}} = 6$ . For all the simulations, the thickness of the sample has been taken as 300  $\mu\text{m}$ , the largest possible to obtain by PLD in a reasonable production time.

### 3. Results

We report a series of simulations performed with the MULTI-FM code. The foam parameters have been chosen as the ones reported in Table 1. We will refer to each simulated nanofoam sample with the corresponding series name reported in that table. As explained in the Methods section, the laser wavelength in the simulations is taken as  $\lambda_L = 1054$  nm. The corresponding critical mass density is, therefore, 3.3 mg/cm<sup>3</sup>, which means that all the foams we are considering are overcritical.

Figure 3 shows the results of the simulations for Series A and B, having both the density of 6 mg/cm<sup>3</sup> and the pore size of 10 and 20  $\mu\text{m}$ , respectively. The shockwave in the nanofoam is slower than in the homogeneous medium. This behavior is well known and theoretically and experimentally documented in the literature for plastic foams [5, 6, 23–25, 29]. It is due to the time required for the laser-generated plasma to homogenize and fill the empty spaces in the foam. The lack of free electrons and the inhomogeneity of the plasma lead to a reduced heat conduction and hydrodynamic motion, until the plasma is homogenized. At that point, the plasma behaves as an ordinary homogeneous plasma.

The characteristic time of homogenization is affected by the pore size  $\delta_0$  as in (6). Because of this dependence, the homogenization time is increased in the case of the nanofoams of Series B, compared to the ones of Series A, and the shockwave is slower in the former than in the latter.

The plots on the right column show that the pressure of the plasma attained in the foam is noticeably higher than that one obtained in the homogeneous medium of the same density. As analytically demonstrated in Ref. [7], an overcritical foam is more efficient than a solid homogeneous material in converting the laser energy into ablation loading. The lower thermal conduction and the inhibited hydrodynamic motion of the cold part of the foam lower the fraction of the laser energy absorbed into the plasma converted into compression or heating of the material. Therefore, a large fraction of this energy is left in the plasma as thermal energy, increasing the pressure in the foam. This property of the foam plasma can be relevant for ICF because it will increase the efficiency of compression on the first inner layer in the fusion target. This feature of foams will be beneficial for ICF, especially considering also the other properties of foam materials, the most important being the high absorption efficiency of the laser energy, which can be as high as 90%.

Figure 4 shows the results of a simulation of a solid-density carbon sample obtained with the MULTI code and with the same equation of state used for the foams, and the density is equal to 2.0 g/cm<sup>3</sup>. The pressure at the shock front

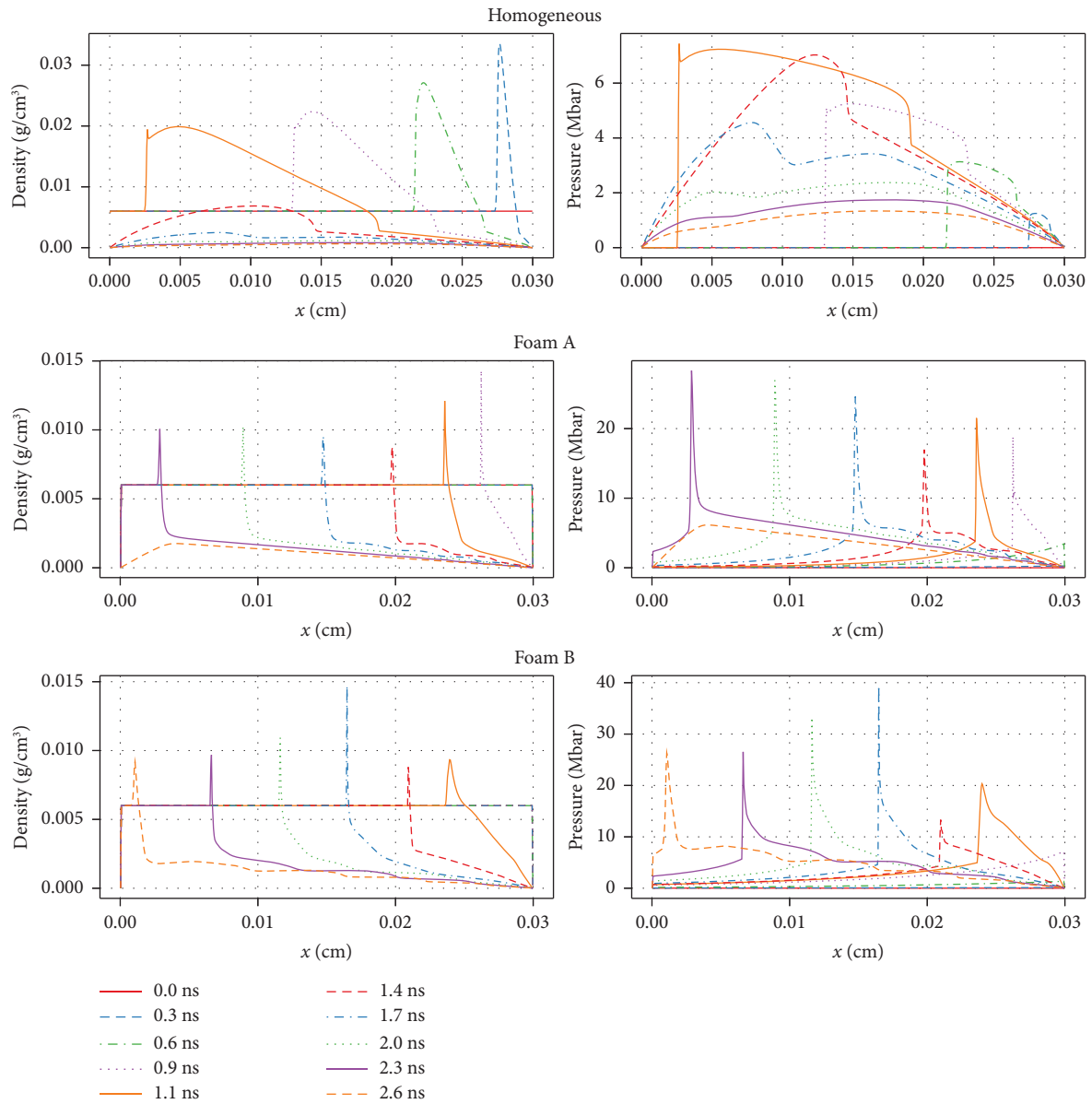


FIGURE 3: The simulations for the homogeneous material and for the nanofoams of cases A and B as in Table 1. The homogeneous material has the same density as the average density of the A and B. The laser comes from the right.

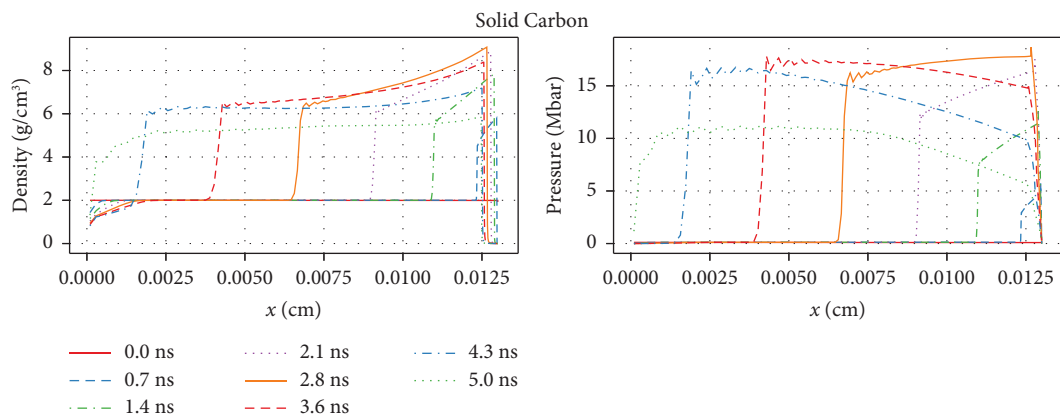


FIGURE 4: The results of simulations with the MULTI code for the case of a sample of solid carbon. The laser comes from the right.

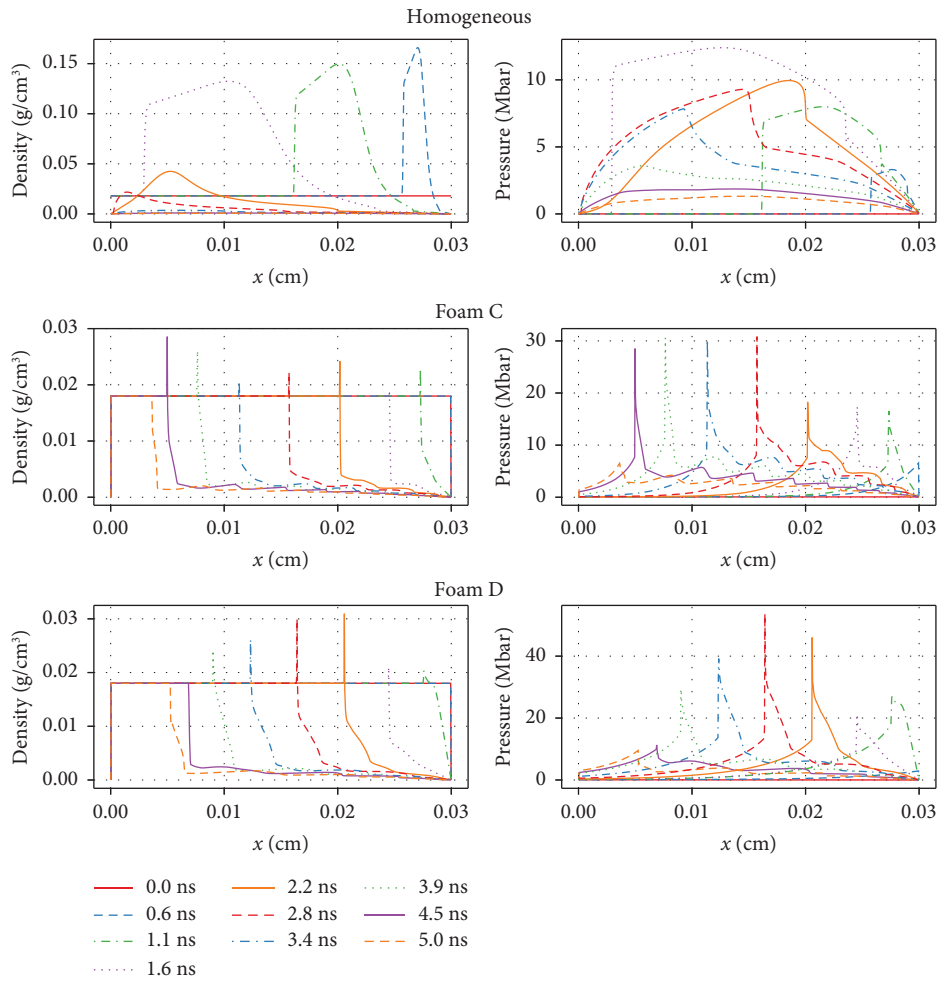


FIGURE 5: The simulations for the homogeneous material and for the nanofoams of cases C and D as in Table 1. The homogeneous material has the same density as the average density of the C and D nanofoams. The laser comes from the right.

in the nanofoam Series A exceeds the pressure obtained in the diamond sample. This effect is even more evident in the case of the nanofoam Series B, where on average it exceeds 20 Mbar.

Figure 5 shows the results of the simulations performed with the nanofoams Series C and D. The oscillations which can be seen in the plots of the density and pressure, in the plasma behind the shock front, are due to the interplay between the homogenization of the plasma and the propagation of the shockwave during the simulation. They reflect the inhomogeneous nature of the plasma realized inside the foam, where some inhomogeneities on large scales are known to remain long after the homogenization time [30]. In nanofoams Series C and D, the shockwave in the foam is slower than in the case of Figure 3. The pore size is smaller, leading to a reduction in the homogenization time, but, at the same time, the density is increased, with the opposite effect (see (6)). The homogenization time is thus mostly unchanged, and the slower shockwave propagation can be attributed to the higher density of the material. The pressure at the shock front in the nanofoam Series C exceeds 20 Mbar on average, an effect even more noticeable in Series D, where it exceeds 30 Mbar.

These results show how a foam can improve the ablation loading, by giving a higher pressure at the front of the shock wave compared with a homogeneous medium. The foams show in all cases a first narrow peak of the pressure at the shock front, followed by a thicker zone of pressure which has generally the same value attained in the homogeneous material. This behavior is related to the limiters in the model, which act on the thermal conductivity and on the compression of the material, reducing both effects (see (8) and (9) in Ref. [23]). The fraction of the plasma energy transformed into the motion of the fluid, and the one transported by heat conduction is reduced in comparison with a homogeneous medium, leading to an increase in the pressure at the front of the shock, which travels at a lower speed.

The simulations can also give an estimate of the most effective choice for the thickness of the sample, to maximize the pressure at the shock front when it exits the ablator. While for Series A, the highest pressure is attained at the end of the laser pulse, in Series B, the peak pressure is reached at 1.7 ns, before the peak power of the laser. By looking at Series C and D, we see that the peak pressure is always reached at about half of the laser time, i.e., when the laser is at its maximum power. Therefore, by properly choosing the



thickness of a carbon nanofoam ablator, depending on the specific laser temporal profile, one can increase the pressure at the shock front and maximize the ablation loading, analogously to what has been observed in Ref. [7] for plastic foams. When considering carbon nanofoams of  $18 \text{ mg/cm}^3$ , for both Series C and D, a thickness of the sample of about  $150 \mu\text{m}$  would be the optimal to improve the compression efficiency from the ablator. Samples with this thickness can easily be obtained with the PLD technique. We will perform dedicated experiments on the ABC facility in the near future to characterize the laser-generated plasma with these nanofoams and to test the results obtained with the MULTI-FM code described in this work.

#### 4. Conclusion

In this work, we reported a first study on the use of carbon nanofoams obtained with the pulsed laser deposition technique as ablators for ICF experiments. We considered four kinds of samples obtained through the use of nanosecond and femtosecond pulsed lasers, reported in Table 1. Taking advantage of the flexibility provided by the two different PLD techniques, two pairs of carbon nanofoams samples with the same average density but different microscale structures (and thus pore size) have been produced: samples A and B with a density of  $6 \text{ mg/cm}^3$  and C and D of  $18 \text{ mg/cm}^3$ . Samples A and C, produced with ns-PLD, have smaller pore size, while larger pore size is obtained for samples B and D, produced with fs-PLD. The nanofoams are characterized in terms of morphology, and a connection between the fractal nanofoam model [15] and the foam description implemented in the MULTI-FM code is proposed. We investigated the behavior of these samples under irradiation of a high-power laser by numerical simulations performed with the MULTI-FM code. In particular, we considered the laser parameters as one of the ABC laser facilities at ENEA Centro Ricerche Frascati. The simulations showed that the shockwave into the nanofoam propagates sensibly slower than in a homogeneous medium of the same average density because of the internal structure of the foam. This effect is enhanced in the case of the nanofoams of Series C and D with an average density of  $18 \text{ mg/cm}^3$  due to the larger average density compared to Series A and B, having an average density of  $6 \text{ mg/cm}^3$ . In all the nanofoams, the pressure at the front of the shockwave is larger than the one obtained in the equivalent homogeneous medium and also higher than the one obtained in a compact carbon sample, whose behavior has been simulated with the same code and equation of state. These first simulations on compact carbon, while limited in scope, are preparatory for future development toward the study of HDC ablators, and the implementation of the proper equation of state into the MULTI-FM code is foreseen. This effect can be of use for realizing an ablator layer for a fusion capsule, increasing the ablation loading on a subsequent layer, thus increasing the compression efficiency. This can be important for direct-drive inertial fusion with carbon-based ablators, such as HDC ablators. Theoretical works showed that mid-Z ablators have a better overall performance than plastic ablators,

also reducing the LPI detrimental effects [12]. The use of carbon nanofoams could improve the performances of fusion targets, combining the benefits that can be obtained from a mid-Z ablator with the ones that come from the use of a porous material, such as the reduction of laser imprint and the smoothing of the laser energy on the capsule. A potential issue related to this finding could reside in the ability of the model implemented in the MULTI-FM code, which presently does not include the possible effects deriving from the interaction of the laser with the peculiar nanoscale structure of the material. Dedicated experiments are foreseen in the near future to confirm the results of this work, through an experimental campaign to be held at the ABC laser facility.

#### Data Availability

The data that support the findings of this study are available from the corresponding authors upon reasonable request.

#### Disclosure

Current address of V. Ciardiello is Università degli Studi del Sannio - Department of Engineering (DING), Piazza Roma, 21 - 82100 Benevento, Italy. Current address of A. Formenti is Accelerator Technology and Applied Physics Division, Lawrence Berkeley National Laboratory, Livermore, CA, USA. Views and opinions expressed are, however, those of the author(s) only and do not necessarily reflect those of the European Union or the European Commission. Neither the European Union nor the European Commission can be held responsible for them. The involved teams have operated within the framework of the Enabling Research Project: ENR-IFE.01.CEA “Advancing shock ignition for direct-drive inertial fusion.”

#### Conflicts of Interest

The authors declare that they have no conflicts of interest.

#### Acknowledgments

This work has been carried out within the framework of the EUROfusion Consortium, funded by the European Union via the Euratom Research and Training Programme (Grant Agreement no. 101052200—EUROfusion).

#### References

- [1] F. Pérez, J. R. Patterson, M. May et al., “Bright x-ray sources from laser irradiation of foams with high concentration of Ti,” *Physics of Plasmas*, vol. 21, no. 2, Article ID 23102, 2014.
- [2] D. Batani, A. Balducci, W. Nazarov et al., “Use of low-density foams as pressure amplifiers in equation-of-state experiments with laser-driven shock waves,” *Physical Review*, vol. 63, no. 4, Article ID 46410, 2001.
- [3] O. N. Rosmej, N. E. Andreev, S. Zaehner et al., “Interaction of relativistically intense laser pulses with long-scale near critical plasmas for optimization of laser based sources of MeV electrons and gamma-rays,” *New Journal of Physics*, vol. 21, no. 4, Article ID 43044, 2019.



- [4] S. Y. Gus'kov, N. V. Zmitrenko, and V. B. Rozanov, "The laser greenhouse thermonuclear target with distributed absorption of laser energy," *Journal of Experimental and Theoretical Physics*, vol. 81, no. 2, pp. 296–305, 1995.
- [5] S. Depierreux, C. Labaune, D. T. Michel et al., "Laser smoothing and imprint reduction with a foam layer in the multikilojoule regime," *Physical Review Letters*, vol. 102, no. 19, Article ID 195005, 2009.
- [6] P. Nicolai, M. Olazabal-Loumé, S. Fujioka et al., "Experimental evidence of foam homogenization," *Physics of Plasmas*, vol. 19, no. 11, Article ID 113105, 2012.
- [7] M. Olazabal-Loumé, P. Nicolai, G. Riazuelo et al., "Simulations of laser imprint reduction using underdense foams and its consequences on the hydrodynamic instability growth," *New Journal of Physics*, vol. 15, no. 8, Article ID 85033, 2013.
- [8] A. E. Bugrov, S. Y. Gus'kov, V. B. Rozanov et al., "Interaction of a high-power laser beam with low-density porous media," *Journal of Experimental and Theoretical Physics*, vol. 84, no. 3, pp. 497–505, 1997.
- [9] M. Cipriani, S. Y. Gus'kov, F. Consoli et al., "Time-dependent measurement of high-power laser light reflection by low-Z foam plasma," *High Power Laser Science and Engineering*, vol. 9, p. e40, 2021.
- [10] R. De Angelis, F. Consoli, S. Y. Gus'kov et al., "Laser-ablated loading of solid target through foams of overcritical density," *Physics of Plasmas*, vol. 22, no. 7, Article ID 72701, 2015.
- [11] M. Hohenberger, D. T. Casey, A. L. Kritcher et al., "Integrated performance of large HDC-capsule implosions on the national ignition facility," *Physics of Plasmas*, vol. 27, no. 11, Article ID 112704, 2020.
- [12] M. Lafon, R. Betti, K. S. Anderson et al., "Direct-drive-ignition designs with mid-Z ablaters," *Physics of Plasmas*, vol. 22, no. 3, Article ID 32703, 2015.
- [13] A. Zani, D. Dellasega, V. Russo, and M. Passoni, "Ultra-low density carbon foams produced by pulsed laser deposition," *Carbon*, vol. 56, pp. 358–365, 2013.
- [14] A. Maffini, A. Pazzaglia, D. Dellasega, V. Russo, and M. Passoni, "Growth dynamics of pulsed laser deposited nanofoams," *Physical Review Materials*, vol. 3, no. 8, Article ID 83404, 2019.
- [15] A. Maffini, D. Orecchia, A. Pazzaglia, M. Zavelani-Rossi, and M. Passoni, "Pulsed laser deposition of carbon nanofoam," *Applied Surface Science*, vol. 599, Article ID 153859, 2022.
- [16] M. Passoni, F. M. Arioli, L. Cialfi et al., "Advanced laser-driven ion sources and their applications in materials and nuclear science," *Plasma Physics and Controlled Fusion*, vol. 62, no. 1, Article ID 14022, 2019.
- [17] I. Prencipe, J. Metzkes-Ng, A. Pazzaglia et al., "Efficient laser-driven proton and bremsstrahlung generation from cluster-assembled foam targets," *New Journal of Physics*, vol. 23, no. 9, Article ID 93015, 2021.
- [18] M. Passoni, A. Sgattoni, I. Prencipe et al., "Toward high-energy laser-driven ion beams: nanostructured double-layer targets," *Physical Review Accelerators and Beams*, vol. 19, no. 6, Article ID 61301, 2016.
- [19] L. Fedeli, A. Formenti, C. E. Bottani, and M. Passoni, "Parametric investigation of laser interaction with uniform and nanostructured near-critical plasmas," *The European Physical Journal D*, vol. 71, no. 8, p. 202, 2017.
- [20] L. Fedeli, A. Formenti, L. Cialfi, A. Sgattoni, G. Cantono, and M. Passoni, "Structured targets for advanced laser-driven sources," *Plasma Physics and Controlled Fusion*, vol. 60, no. 1, Article ID 14013, 2017.
- [21] A. Maffini, F. Mirani, M. Galbiati et al., "Towards compact laser-driven accelerators: exploring the potential of advanced double-layer targets," *EPJ Techn Instrum*, vol. 10, no. 1, p. 15, 2023.
- [22] A. Pazzaglia, L. Fedeli, A. Formenti, A. Maffini, and M. Passoni, "A theoretical model of laser-driven ion acceleration from near-critical double-layer targets," *Communications Physics*, vol. 3, no. 1, p. 133, 2020.
- [23] M. Cipriani, S. Y. Gus'kov, R. De Angelis et al., "Laser-supported hydrothermal wave in low-dense porous substance," *Laser and Particle Beams*, vol. 36, no. 1, pp. 121–128, 2018.
- [24] M. Cipriani, S. Y. Gus'kov, R. De Angelis et al., "Laser-driven hydrothermal wave speed in low-Z foam of overcritical density," *Physics of Plasmas*, vol. 25, no. 9, Article ID 92704, 2018.
- [25] J. Velechovsky, J. Limpouch, R. Liska, and V. Tikhonchuk, "Hydrodynamic modeling of laser interaction with microstructured targets," *Plasma Physics and Controlled Fusion*, vol. 58, no. 9, Article ID 95004, 2016.
- [26] A. Pazzaglia, A. Maffini, D. Dellasega, A. Lamperti, and M. Passoni, "Reference-free evaluation of thin films mass thickness and composition through energy dispersive x-ray spectroscopy," *Materials Characterization*, vol. 153, pp. 92–102, 2019.
- [27] A. Maffini, A. Pazzaglia, D. Dellasega, V. Russo, and M. Passoni, "Production of carbon nanofoam by pulsed laser deposition on flexible substrates," in *Nanoporous Carbons for Soft and Flexible Energy Devices*, pp. 135–157, Springer, Berlin, Germany, 2022.
- [28] R. Ramis, R. Schmalz, and J. Meyer-Ter-Vehn, "Multi—a computer code for one-dimensional multigroup radiation hydrodynamics," *Computer Physics Communications*, vol. 49, no. 3, pp. 475–505, 1988.
- [29] V. T. Tikhonchuk, T. Gong, N. Jourdain et al., "Studies of laser-plasma interaction physics with low-density targets for direct-drive inertial confinement fusion on the Shenguang III prototype," *Matter and Radiation at Extremes*, vol. 6, no. 2, Article ID 25902, 2021.
- [30] J. Limpouch, V. T. Tikhonchuk, J. Dostál et al., "Characterization of residual inhomogeneities in a plasma created by laser ionization of a low-density foam," *Plasma Physics and Controlled Fusion*, vol. 62, no. 3, Article ID 35013, 2020.